

Geometric Analysis of Blind User Identification for Massive MIMO Networks

Levi Bohnacker, Ralf R. Müller
 FAU Erlangen-Nürnberg
 Institute for Digital Communications
 D-91058 Erlangen, Germany
 emails: {levi.bohnacker, ralf.r.mueller}@fau.de

Abstract—Applying Nearest Convex Hull Classification (NCHC) to blind user identification in a massive Multiple Input Multiple Output (MIMO) communications system is proposed. The method is blind in the way that the Base Station (BS) only requires a training sequence containing unknown data symbols obtained from the user without further knowledge on the channel, modulation, coding or even noise power. We evaluate the algorithm under the assumption of gaussian transmit signals using the non-rigorous replica method. To facilitate the computations the existence of an Operator Valued Free Fourier Transform is postulated, which is verified by Monte Carlo simulation. The replica computations are conducted in the large but finite system by applying saddle-point integration with inverse temperature β as the large parameter. The classifier accuracy is estimated by gaussian approximation through moment-matching.

I. INTRODUCTION

Future communication networks are envisioned to enable a multitude of applications through one physical network. First realizations of such concepts are observed in 5G Network Slices (NS) which enable to partition the network into virtual sub-networks providing low-latency or high data rates [1]. Application oriented slicing is envisioned for 6G, e.g. in the context of Artificial Intelligence (AI) applications [2]. At the same time, MIMO is a key enabler of the ever growing demand for high data rates, user density and reliability.

In this work, a massive MIMO network in which two proprietary applications (a and b) share one radio frequency (RF)-chain/BS is considered. We assume that the users transmit to the base station at random through a multiple-access scheme mitigating collisions on the network, i.e. no two users transmit at the same time. The two networking applications do not reveal the applied modulation and coding scheme or observed Channel-State-Information (CSI) and Signal-to-Noise Ratio (SNR) to the BS. To forward the received signal to the correct application without leaking information intend for application a to b , or vice versa, a blind classifier is applied on the signal received at the BS. To train the classifier, each user sends a burst of N transmissions along with some application identifier upon synchronization to the BS. We observe that this training sequence can be interpreted as noisy samples of a convex hull in high-dimensional space. Based on this intuition we propose to apply a Nearest Convex Hull Classifier (NCHC) [3] for blind user identification. The NCHC is computationally expensive in the large dimensional regime and hence subject to theoretical analysis only, from which we can draw insights into the fundamental underlying problem. Practical implementations may utilize Approximate NCHC (ANCHC) such as the algorithm proposed in [4]. An empiric comparison of the ANCHC and NCHC in the proposed framework is subject to future work. Asymptotic analysis of the NCHC is carried out by replica

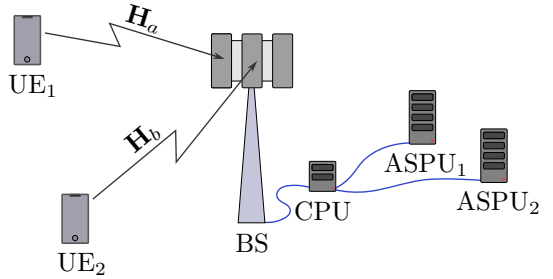


Fig. 1: System architecture: two users communicating through one BS to user-specific, secure applications.

method [5]. We compare the obtained results with Monte Carlo simulations, showing that the replica computations are precise. In order to characterize the NCHC, two spin glasses are defined and analyzed in an *isolated* and a *coupled* setting. The coupling induces a spherical integral which can be seen as a modified operator-valued version of the famous Harish-Chandra-Itzykson-Zuber (HCIZ) integral [6], [7]. To solve the integral asymptotically, a generalization of the Free Fourier Transform [8] to the operator valued case is postulated, which is to the best of the authors knowledge a novel result. An additional modification of the (operator valued) HCIZ integral and the corresponding asymptotics enables the averaging operations during replica computation.

II. PROBLEM FORMULATION

A. System Model

Consider a communication system comprised of two user equipments (UEs): $UE_k \forall k \in \{a, b\}$; and one BS. The UEs as well as the BS are equipped with M antennas each. The BS RF-chain feeds into a Central Processing Unit (CPU) which handles the user classification and maps the received signal to the corresponding Application Specific Processing Unit (ASPU) *without* demodulation, as shown in Fig. 1. Upon initial setup and synchronization, UE_k transmits a burst of N vector-valued symbols $\mathbf{x}_i \in \mathbb{R}^{M \times 1} \forall i \in \{1, \dots, N\}$. The corresponding received signal at the BS is given by:

$$\mathbf{Y}_k = \frac{1}{\sqrt{M}} \mathbf{H}_k \mathbf{X}_k + \sigma \mathbf{N}_k \quad (1)$$

where $\mathbf{H}_k = (h_{k,i,j})_{i,j=1}^M$ models the channel, $\mathbf{N}_k = (n_{k,i,j})_{i,j=1}^{M,N}$ models *independent identical distributed (i.i.d.)* Additive White Gaussian Noise (AWGN) of zero mean and unit variance: $n_{k,i,j} \sim \mathcal{N}(0, 1)$ and $\mathbf{X}_k = [\mathbf{x}_{k,1}, \dots, \mathbf{x}_{k,N}] \in \mathbb{R}^{M \times N}$ is the matrix-valued transmit signal. The channel as well as the transmit symbols are modeled by *i.i.d* gaussian coefficients of zero mean and unit variance: $h_{k,i,j} \sim \mathcal{N}(0, 1)$, $\mathbf{x}_{k,i} \sim \mathcal{N}(0, \mathbb{I}_M)$ where $\mathbb{I}_M \in \mathbb{R}^{M \times M}$ is the $M \times M$ identity matrix.

Upon reception of the training sequences \mathbf{Y}_a and \mathbf{Y}_b the BS knows that there are two users in the system associated to application a and b . The BS does not have any knowledge of the noise power, signal power or even the underlying system model in (1). Given an unseen received signal \mathbf{y}_0 (2), the BS classifies the application/user based on the received training sequences only.

$$\mathbf{y}_0 = \frac{1}{\sqrt{N}} \mathbf{H}_l \mathbf{x}_0 + \sigma \mathbf{n}_0 \quad (2)$$

In the following we give intuition for why the training sequence forms a convex hull in M -dimensional space.

B. An Intuition for Convex Hulls

According to the *Law of Large Numbers* (LLN), the normalized squared $L2$ -norm of a high-dimensional *i.i.d.* gaussian vector converges to its variance. It is hence intuitive, that all columns of $\frac{1}{\sqrt{M}} \mathbf{X}_k$ lie on the $(M - 1)$ -sphere as illustrated in Fig.2 (a). Upon transmission through the channel, these gaussian vectors are reshaped in accordance to the singular value distribution of $\frac{1}{\sqrt{M}} \mathbf{H}_k$ which is described by the Marčenko-Pastur Law at $\zeta = 1$ [9], also known as the Quarter Circle Law [10]. As some singular values are larger than others the hyper-sphere is reshaped to an ellipsoid upon transmission through the channel. The AWGN of power σ^2 shifts samples of the ellipsoid to lie on $(M - 1)$ -spheres centered around $\frac{1}{M} \mathbf{H}_a \mathbf{x}_{a,i}$, as shown in Fig.2 (b). Let the training sequence length $N \rightarrow \infty$. The additive noise induces a sample distribution centered around the contour of the ellipsoid defined by $\frac{1}{\sqrt{M}} \mathbf{H}_k$, see Fig.2 (c). The width of this 'belt' approaches 2σ as $M \uparrow \infty$.

We interpret the noisy ellipsoid as the typical set of received signals. For sufficiently large N , the NCHC compares a new sample to the contour of the ellipsoid, effectively applying typical set decoding. This motivates us to analyze the underlying geometry by means of NCHC.

C. Nearest Convex Hull Classifier

The convex hull around a training sequence \mathbf{Y}_k describes any point $\tilde{\mathbf{y}}$ which can be reached by a convex combination of all samples in \mathbf{Y}_k . The set of all these points is identified by $\text{Conv}(\mathbf{Y}_k)$:

$$\text{Conv}(\mathbf{Y}_k) = \left\{ \sum_{i=1}^N \mathbf{y}_{k,i} v_i \mid \|\mathbf{v}\|_1 = 1, \mathbf{v} \in [0, 1]^N \right\} \quad (3)$$

with $\mathbf{Y}_k = [\mathbf{y}_{k,1}, \dots, \mathbf{y}_{k,N}]$. Two training sequences \mathbf{Y}_a and \mathbf{Y}_b form two distinct convex hulls. The NCHC classifies a received signal \mathbf{y}_0 by assigning it to the application for which the corresponding convex hull is closer. The squared Euclidean distance of \mathbf{y}_0 to $\text{Conv}(\mathbf{Y}_k)$ is computed by the following convex optimization problem:

$$\begin{aligned} D_{l;k} = \min_{\mathbf{v} \in [0, 1]^N} \quad & \|\mathbf{y}_0 - \mathbf{Y}_k \mathbf{v}\|_2^2 \\ \text{s.t.} \quad & \|\mathbf{v}\|_1 = 1 \end{aligned} \quad (4)$$

where $l \in \{a, b\}$ identifies the class to which \mathbf{y}_0 belongs. We identify $l = k$ as the Direct Hull (DH) case, i.e. the training sequence and received symbol belong to the same hull and $l \neq k$ as the Cross Hull (CH) case. In the binary class case we can define a simple decision metric: $D_l = D_{l;a} - D_{l;b}$. If $D_l < 0$, the test point is classified as a and otherwise as

b. Assuming a uniform prior, we set $l = a$ without loss of generality. The classifier accuracy is defined by:

$$\text{AC}_a(\{\mathbf{Y}_k\}) = \mathcal{E}_{\mathbf{y}_0 \mid l=a} \{\mathbb{1}(D_a < 0)\} \quad (5)$$

$$= \Pr(D_a < 0 \mid l = a, \{\mathbf{Y}_k\}) \quad (6)$$

where $\mathbb{1}(\cdot)$ is the indicator function, $\{\mathbf{Y}_k\}$ identifies \mathbf{Y}_a and \mathbf{Y}_b and $\mathcal{E}_{x \mid y} \{\cdot\}$ is the expectation operation with respect to (w.r.t.) x given y . We aim to compute the average accuracy over all possible channel realizations \mathbf{H}_k , transmit training sequences \mathbf{X}_k , noise realizations \mathbf{N}_k and received signals \mathbf{y}_0 :

$$\overline{\text{AC}_a} = \overline{\mathcal{E}_{\mathbf{y}_0, \{\mathbf{Y}_k\} \mid l=a} \{\mathbb{1}(D_a < 0)\}} \quad (7)$$

where \overline{X} signifies the average of X over all random variables contained in X .

III. THE REPLICA COMPUTATIONS

A. Replica Ansatz

The replica method is a tool from statistical physics which allows to analyze large systems in the thermodynamic equilibrium [5]. While it is known to miss mathematical rigor, applying the replica method produces results which closely follow numerical simulations and have been shown to be rigorous in certain cases. We apply the replica method to solve the expectation over the accuracy metric (7). This however is not straightforward as we will be unable to find an analytic continuation around the replica parameter t for $t > 0$. Instead we leverage Gaussian approximation through moment-matching, computing the mean (8) and variance (9) of the decision metric by replica method.

$$\overline{D_a} = \overline{D_{a;a}} - \overline{D_{a;b}} \quad (8)$$

$$\begin{aligned} \text{Var}(D_a) &= \overline{(D_{a;a} - D_{a;b})^2} - \overline{D_{a;a} - D_{a;b}}^2 \\ &= 2\text{Var}(D_{a;a}) + 2\text{Var}(D_{a;b}) - \text{Var}(D_{a;a} + D_{a;b}) \end{aligned} \quad (9)$$

The spin glass energy function is defined in a general setting by the Hamiltonian (10).

$$\begin{aligned} \mathcal{H}(\mathbf{v}_a, \mathbf{v}_b \mid \{\mathbf{Y}_i\}, \mathbf{y}_0) &= \tau_a \|\mathbf{y}_0 - \mathbf{Y}_a \mathbf{v}_a\|_2^2 \\ &+ \tau_b \|\mathbf{y}_0 - \mathbf{Y}_b \mathbf{v}_b\|_2^2 \end{aligned} \quad (10)$$

Parameters $\tau_a, \tau_b \in \{0, 1\}$ allow to combine the DH and CH terms. Selecting $\tau_a = \tau_b = 1$ is referred to as the *coupled* spin glass whereas $\tau_a \neq \tau_b$ yields an *isolated* spin glass. To reduce notational overhead we identify all random variables by Ω . The corresponding free energy is given by:

$$F(\beta \mid \Omega) = -\frac{1}{\beta M} \log \int d\mathbf{v}_a d\mathbf{v}_b e^{-\beta \mathcal{H}(\mathbf{v}_a, \mathbf{v}_b \mid \Omega)} \delta_{\|\mathbf{v}_a\|_1} \delta_{\|\mathbf{v}_b\|_1} \quad (11)$$

$$= -\frac{1}{\beta M} \log Z(\beta \mid \Omega) \quad (12)$$

The integral is taken on the domains $\mathbf{v}_a, \mathbf{v}_b \in [0, 1]^{N \times 1}$, $\delta_{\|\mathbf{v}_k\|_1} = \delta(\|\mathbf{v}_k\|_1 - 1)$ enforces the unit $L1$ -norm constraint on the two microstate variables \mathbf{v}_a and \mathbf{v}_b , $Z(\beta \mid \Omega)$ is the partition function and β is the inverse temperature parameter. In order to obtain the statistics of the free energy we define the Scaled Cumulant Generating Function (SCGF) (14).

$$G(\beta, t) = -\frac{1}{\beta M} \log \overline{Z(\beta \mid \Omega)^t} \quad (13)$$

$$= -\frac{1}{\beta M} \log \overline{e^{-t \beta M F(\beta \mid \Omega)}} \quad (14)$$

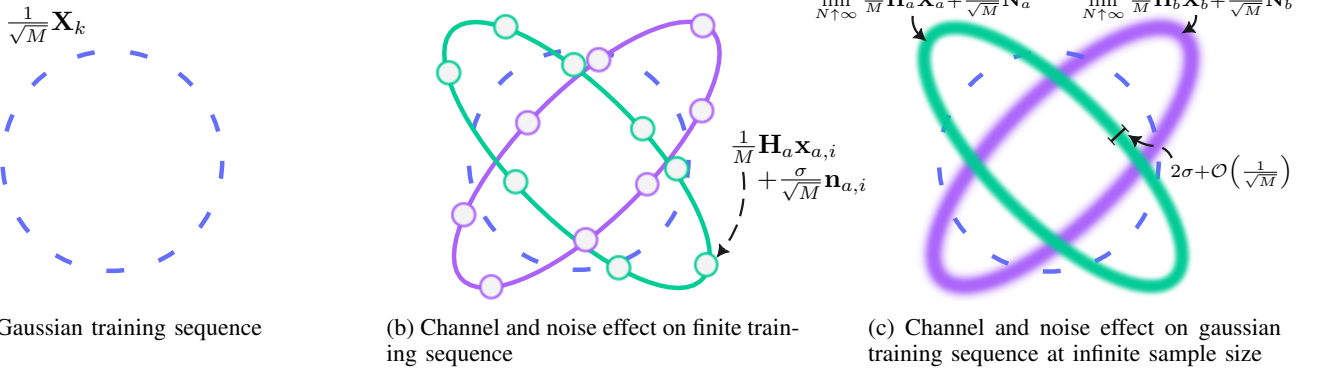


Fig. 2: Illustration of the geometry of a high-dimensional training sequence normalized with $\frac{1}{\sqrt{M}}$

The first and second order derivative of (14) w.r.t. t at $t = 0$ yields the mean and scaled variance of the free energy, respectively:

$$\frac{\partial}{\partial t} G(\beta, t) \Big|_{t=0} = \overline{F(\beta|\Omega)} \quad (15)$$

$$\frac{\partial^2}{\partial t^2} G(\beta, t) \Big|_{t=0} = -\beta M \left(\overline{F(\beta|\Omega)^2} - \overline{F(\beta|\Omega)}^2 \right) \quad (16)$$

As the spin glass freezes: $\beta \uparrow \infty$; the integral in (11) is solved by saddle-point integration where the extrema of the exponent correspond to the solution of (4). Computing the free energy cumulants at inverse temperature $\beta \uparrow \infty$ hence provides the cumulants of the decision metric D_a . Obtaining a closed form solution to the SCGF $G(\beta, t)$ therefore facilitates the computation of (15) and (16). The following paragraphs outline the replica computations corresponding to the isolated and coupled spin glass, respectively.

B. The Isolated Spin Glasses

The CH and DH isolated spin glasses are not identical. We hence present a generalized approach parametrized by $k = a$ on $\tau_a = 1$ (DH) and $k = b$ on $\tau_b = 1$ (CH). Explicit analytic function forms are omitted, in order to reduce notational overhead. The averaged replicated partition function of the isolated spin glass is denoted by $f_{Z,k}(\beta, t) \forall k \in \{a, b\}$ and referred to as the isolated moments function.

$$f_{Z,k}(\beta, t) = \int \mathcal{E}_\Omega \left\{ e^{-\beta \sum_{r=1}^t \|\mathbf{H}_a \mathbf{x}_0 + \sigma \mathbf{n}_0 - (\mathbf{H}_k \mathbf{x}_k + \mathbf{N}_k) \mathbf{v}_{k,r}\|_2^2} \right\} \times \prod_{r=1}^t \delta_{\|\mathbf{v}_{k,r}\|} d\mathbf{v}_{k,r} \quad (17)$$

In a first step, the average over \mathbf{N}_k is computed by gaussian integration. Then, we jointly average over \mathbf{x}_0 and \mathbf{n}_0 by interpreting \mathbf{y}_0 as a multivariate Gaussian of zero-mean and covariance $\mathbf{C}_{\mathbf{y}_0} = \sigma^2 \mathbb{I}_M + \frac{1}{M} \mathbf{H}_a \mathbf{H}_a^T$. This two-fold gaussian integration yields:

$$f_{Z,k}(\beta, t) = \int \mathcal{E}_{X,H} \left\{ e^{-\beta \alpha N \sum_{r=1}^t \text{tr} \{ \mathbf{D}_{k,r} \tilde{\mathbf{X}}_k^T \mathbf{A}_{k,r} \tilde{\mathbf{X}}_k \} + \mathcal{D}(\mathbf{\Lambda}_k)} \right\} \times \prod_{r=1}^t \delta_{\|\mathbf{v}_{k,r}\|} d\mathbf{v}_{k,r} \quad (18)$$

where $\alpha = \frac{M}{N}$, $\mathbf{\Lambda}_k$ is a diagonal $N \times N$ matrix containing the eigenvalues of $\mathbf{V}_k \mathbf{V}_k^T$, $\mathbf{D}_{k,r}$ is a rank-one diagonal matrix with a non-zero entry θ_r at index (r, r) which is a function of the r^{th} eigenvalue of $\mathbf{V}_k \mathbf{V}_k^T$, $\tilde{\mathbf{X}}_k = \frac{1}{\sqrt{M}} \mathbf{U} \mathbf{X}_k$ and $\mathbf{A}_{k,r}$ is a function of $\frac{1}{\sqrt{M}} \mathbf{H}_k$, σ , β and $\mathbf{V}_k \mathbf{V}_k^T$. With $\mathbf{V}_k = [\mathbf{v}_{k,1}, \dots, \mathbf{v}_{k,t}] \in [0, 1]^{N \times t}$. Furthermore, the function

$\mathcal{D} : \mathbb{R}^{N \times N} \rightarrow \mathbb{R}$ is induced by the covariance scaling of the gaussian integral and is self-averaging w.r.t. \mathbf{H}_a . The empirical singular-value spectrum (ESD) of $\tilde{\mathbf{X}}_k$ and $\mathbf{A}_{k,r}$ converges and is bounded. We hence only have to average over the left unitary matrix of the Singular Value Decomposition (SVD) of $\tilde{\mathbf{X}}_k$ which is distributed by a Haar measure on the orthogonal group: $\mu(\cdot)$.

$$\Xi_{X,k} = \int \exp \left\{ -\beta \alpha N \sum_{r=1}^t \theta_r \mathbf{u}_{k,r}^T \tilde{\mathbf{X}}_k^T \mathbf{A}_{k,r} \tilde{\mathbf{X}}_k \mathbf{u}_{k,r} \right\} d\mu(\mathbf{U}_k) \quad (19)$$

with $\mathbf{U}_k = [\mathbf{u}_{k,1}, \dots, \mathbf{u}_{k,t}]$ and $\Xi_{X,k}$ being a symbolism for the expectation over \mathbf{X}_k . The integral (19) is a spherical integral. In fact, if $\mathbf{A}_{k,r} = \mathbf{A}_k \forall r$ were to hold, this would be a reformulation of the well known HCIZ integral [6], [7], which is solved asymptotically in the low-rank regime using the Free Fourier Transform [8]. By modifying the derivations in [8], we allow the inner matrix $\mathbf{A}_{k,r}$ to be dependent on the index r such that:

$$\Xi_{X,k} \doteq e^{-\beta \alpha N \sum_{r=1}^t \int_0^1 \theta_r R_{\tilde{\mathbf{X}}_k^T \mathbf{A}_{k,r} \tilde{\mathbf{X}}_k}(-2\beta\alpha\theta_r w) dw} \quad (20)$$

where \doteq signifies asymptotic equivalence and $R_{\mathbf{B}}(\cdot)$ is the R-transform of \mathbf{B} [11]. Considering that θ_r is a function of the r^{th} eigenvalue of $\mathbf{V}_k \mathbf{V}_k^T = \mathbf{G}(\{\mathbf{v}_{k,r}\})$, (20) is given in matrix notation by (21).

$$\Xi_{X,k} \doteq e^{-\beta \alpha N \int_0^1 \text{tr} \{ \mathbf{G}(\{\mathbf{v}_{k,r}\}) R_{k,\{r\}}(-2\beta\alpha w \mathbf{G}(\{\mathbf{v}_{k,r}\})) \}} \quad (21)$$

The matrix valued function $R_{k,\{r\}}$ applies the R-transform $R_{\tilde{\mathbf{X}}_k^T \mathbf{A}_{k,r} \tilde{\mathbf{X}}_k}(\cdot)$ to the r^{th} eigenvalue of its argument. In (21), $\Xi_{X,k}$ is fully characterized by the eigenvalues of $\mathbf{G}(\{\mathbf{v}_{k,r}\}) \in [0, 1]^{N \times N}$. As these are identical to the eigenvalues of $\mathbf{Q}(\{\mathbf{v}_{k,r}\}) = \mathbf{V}_k^T \mathbf{V}_k \in \mathbb{R}^{t \times t}$, Ξ_X can be expressed as a function of this *replica correlation* matrix. To simplify the integral over $\{\mathbf{v}_{k,r}\}$, the subshell (22) is defined.

$$\mathbf{S}(\mathbf{Q}_k) = \{(\mathbf{v}_{k,1}, \dots, \mathbf{v}_{k,t} | \mathbf{v}_{k,t}^T \mathbf{v}_{k,j} = q_{k,ij})\} \quad (22)$$

with $\mathbf{Q}_k = (q_{k,i,j})_{i,j=1}^t$. By subshell integration of (17) after averaging over Ω , the moments function (23) is obtained.

$$f_{Z,k}(\beta, t) = \int d\mathbf{Q}_k e^{-\mathcal{K}_k(\mathbf{Q}_k) - \mathcal{D}(\mathbf{Q}_k) + \mathcal{I}(\mathbf{Q}_k)} \quad (23)$$

with:

$$\mathcal{K}_k(\mathbf{Q}_k) = \beta \alpha N \int_0^1 \text{tr} \{ \mathbf{Q}_k R_{k,\{r\}}(-2\beta\alpha w \mathbf{Q}_k) \} dw \quad (24)$$

$$\begin{aligned} \mathcal{D}(\mathbf{Q}_k) = & \frac{M}{2} \log |\mathbb{I}_t + 2\beta\sigma^2 \mathbf{Q}_k| + \frac{1}{2} \log |\sigma^2 \mathbb{I}_M + \mathbf{H}_a \mathbf{H}_a^T| \\ & + \frac{1}{2} \log |(\sigma^2 \mathbb{I}_M + \mathbf{H}_a \mathbf{H}_a)^{-1} + e(\mathbf{Q}_k) \mathbb{I}_b| \end{aligned} \quad (25)$$

and the subshell density $\mathcal{I}(\mathbf{Q}_k)$:

$$\begin{aligned}\mathcal{I}(\mathbf{Q}_k) &= \log \int \delta(\mathbf{Q} - \mathbf{V}_k^T \mathbf{V}_k) \prod_{r=1}^t \delta_{\|\mathbf{v}_{k,r}\|_1} d\mathbf{v}_{k,r} \quad (26) \\ &= \log \int \delta(\beta \mathbf{Q} - \beta \mathbf{V}_k^T \mathbf{V}_k) \prod_{r=1}^t \delta(\beta \|\mathbf{v}_{k,r}\|_1 - \beta) d\mathbf{v}_{k,r} \\ &\quad + (t+1) \log(\beta) \quad (27)\end{aligned}$$

Averaging over \mathbf{H}_a is not done explicitly as the log-determinants are self-averaging at large N and M . To compute the sub-shell density we follow the approach taken in [12] and obtain (28). The summand $(t+1) \log(\beta)$ is ignored in subsequent steps as it will vanish for large β upon normalization with $\frac{1}{\beta}$ in (11).

$$e^{\mathcal{I}(\mathbf{Q}_k)} = \int d\mathbf{S}_k d\mathbf{r}_k e^{-\beta \text{tr}\{\mathbf{S}_k^T \mathbf{Q}_k\} - \beta \mathbf{r}_k^T \mathbf{1}_{t \times 1} + \mathcal{P}(\mathbf{S}_k, \mathbf{r}_k)} \quad (28)$$

with:

$$\mathcal{P}(\mathbf{S}_k, \mathbf{r}_k) = N \log \int_{\mathbf{v} \in [0,1]^t} \exp \{\beta \mathbf{v}^T \mathbf{S}_k \mathbf{v} + \beta \mathbf{r}_k^T \mathbf{v}\} d\mathbf{v} \quad (29)$$

Replica-Symmetry (RS) parametrization is applied to $\mathbf{Q}_k, \mathbf{S}_k$ and \mathbf{r}_k .

$$\mathbf{Q}_k = \frac{\chi_k}{\beta} \mathbb{I}_t + q_k \mathbf{1}_{t \times t} \quad (30)$$

$$\mathbf{S}_k = -e_k \mathbb{I}_t + \frac{\beta f_k^2}{2} \mathbf{1}_{t \times t} \quad (31)$$

$$\mathbf{r}_k = r_k \mathbf{1}_{t \times 1} \quad (32)$$

RS parametrization of $\mathcal{K}_k(\mathbf{Q}_k)$ and $\mathcal{P}(\mathbf{S}_k, \mathbf{r}_k)$ does not admit an analytic solution for $t > 0$ on the real line. By Taylor expansion around $t = 0$, the terms can be sufficiently approximated up to order t^2 . Computing higher order terms is possible but tedious, especially for $\mathcal{K}_k(\mathbf{Q}_k)$. The computations reveal that any integer power of the inverse temperature $\beta^i \forall i \in \mathbb{Z}^+$ is scaled by a corresponding t^i . Where \mathbb{Z}^+ is the set of positive integer numbers excluding 0. The RS parametrized exponents can therefore be sorted by their scaling in β (33).

$$f_{Z,k}^{\text{RS}}(\beta, t) \propto \int e^{-t\mathcal{B}_k^{(0)} - t\beta\mathcal{B}_k^{(1)} - t^2\beta^2\mathcal{B}_k^{(2)} + \Omega(t^3)} dP_k^{\text{RS}} \quad (33)$$

The terms $\mathcal{B}_k^{(i)}$ are functions of the RS parameters χ_k, q_k, e_k, f_k and r_k and dP_k^{RS} indicates integration over all said parameters. In order to compute the first and second cumulant of the decision metrics, (15) and (16) are evaluated at $\beta \uparrow \infty$. Equation (34) states the first cumulant after differentiating the SCGF $G(\beta, t)$ w.r.t. t .

$$\begin{aligned}\frac{D_{a;k}}{M} &= \lim_{\beta \uparrow \infty} \lim_{t \downarrow 0} \frac{1}{M} \int \frac{\frac{\mathcal{B}_k^{(0)}}{\beta} + \mathcal{B}_k^{(1)} + 2t\beta\mathcal{B}_k^{(2)} + \Omega(t^2)}{\int e^{-t\mathcal{B}_k^{(0)} - t\beta\mathcal{B}_k^{(1)} - t^2\beta^2\mathcal{B}_k^{(2)} + \Omega(t^3)} dP_k^{\text{RS}}} \\ &\quad \times e^{-t\mathcal{B}_k^{(0)} - t\beta\mathcal{B}_k^{(1)} - t^2\beta^2\mathcal{B}_k^{(2)} + \Omega(t^3)} dP_k^{\text{RS}} \quad (34)\end{aligned}$$

Typically, the integral in (34) is solved in the limit $M \uparrow \infty$. In this case however not all terms scale with M due to the finite-value constraint on the $L1$ -Norm of the microstate: $\delta_{\|\mathbf{v}\|_1}$. We merely enforce large *but finite* M, N such that the asymptotic equalities hold with sufficient accuracy. Using a non-rigorous reordering of the limits, saddle-point integration is applied with β as the large parameter. In order to facilitate the limit exchange, we omit all exponent terms in $\Omega(t^2)$ as they vanish fast enough for small t . Additionally we omit all scaling terms

in $\Omega(t)$ as their contribution vanishes for $t \downarrow 0$ and there are no exponent terms in $\mathcal{O}(\frac{1}{t})$. The contribution of $\mathcal{B}_k^{(0)}$ grows insignificant at large β and can hence be neglected in (35) with vanishing error.

$$\frac{1}{M} \overline{D_{a;k}} = \lim_{t \downarrow 0} \lim_{\beta \uparrow \infty} \frac{1}{M} \int \mathcal{B}_k^{(1)} \frac{\exp\{-t\beta\mathcal{B}_k^{(1)}\}}{\int \exp\{-t\beta\mathcal{B}_k^{(1)}\} dP_k^{\text{RS}}} dP_K^{\text{RS}} \quad (35)$$

The fraction in (35) admits a *Boltzmann-Gibbs distribution* with Hamiltonian $t\mathcal{B}_k^{(1)}$ and hence exhibits a ground-state property at $\beta \uparrow \infty$. The integral is asymptotically solved in (36).

$$\frac{1}{M} \overline{D_{a;k}} = \frac{1}{M} \mathcal{B}_k^{(1)}(\chi_k^*, q_k^*, e_k^*, f_k^*, r_k^*) \quad (36)$$

Where $\chi_k^*, q_k^*, e_k^*, f_k^*$ and r_k^* are the RS parameters at the extrema of $\mathcal{B}_k^{(1)}$, which is attained by setting all partial derivatives w.r.t. to the RS parameters to zero. The variance (37) is obtained in a similar fashion, starting from the second order derivative of (33) w.r.t. t .

$$\text{Var} \left(\frac{1}{M} D_{a;k} \right) = -\frac{2}{M^2} \mathcal{B}_k^{(2)}(\chi_k^*, q_k^*, e_k^*, f_k^*, r_k^*) \quad (37)$$

The extrema RS parameters of (36) and (37) are identical.

C. The Coupled Spin Glass

The sum variance $\text{Var}(D_{a;a} + D_{a;b})$ is computed by *coupling* the spin glasses: $\tau_a = \tau_b = 1$. The gaussian integrals remain virtually identical up to some minor changes in the determinant terms (25). It is only in the expectation over \mathbf{X}_a and \mathbf{X}_b (38) that the coupling is characterized by matrix \mathbf{C}_{12} , a function of $\tilde{\mathbf{X}}_a$ and $\tilde{\mathbf{X}}_b$.

$$\begin{aligned}\Xi_X &= \int \int e^{-\alpha N \theta_{a,1} \mathbf{u}_{a,1}^T \mathbf{C}_{11} \mathbf{u}_{a,1} - 2\alpha N \sqrt{\theta_{a,1} \theta_{b,1}} \mathbf{u}_{a,1}^T \mathbf{C}_{12} \mathbf{u}_{b,1}} \\ &\quad \times e^{-2\alpha N \theta_{b,1} \mathbf{u}_{b,1}^T \mathbf{C}_{22} \mathbf{u}_{b,1}} \\ &\quad \times e^{-\alpha N \sum_k \sum_{r=2}^t \theta_{k,2} \mathbf{u}_{k,r}^T \tilde{\mathbf{X}}_k \mathbf{H}_k \mathbf{H}_k \tilde{\mathbf{X}}_k \mathbf{u}_{k,r}} d\mu(\mathbf{U}_a) d\mu(\mathbf{U}_b) \quad (38)\end{aligned}$$

where \mathbf{C}_{11} and \mathbf{C}_{22} are functions of $\tilde{\mathbf{X}}_a$ and $\tilde{\mathbf{X}}_b$, respectively. This spherical integral can be interpreted as a set of *modified* (in the sense of (19)) HCIZ integrals coupled through \mathbf{C}_{12} . The derivations to solve (38) are omitted due to space constraints. Instead we present our result as a proposition followed by two claims. We have obtained a partial proof of the proposition, the claims are based on the results of [8] and the corresponding modification used in the isolated spin glass computation.

Proposition 1 (Rank-1 Operator Valued Free Fourier Transform): Consider a spherical integral of the form:

$$I_N(\{\theta_k\}, \mathbf{Z}) = \int \int e^{-N \theta_a \mathbf{u}_{a,1}^T \mathbf{C}_{11} \mathbf{u}_{a,1} - N \theta_b \mathbf{u}_{b,1}^T \mathbf{C}_{22} \mathbf{u}_{b,1}} \\ \times e^{-2N \sqrt{\theta_a \theta_b} \mathbf{u}_{a,1}^T \mathbf{C}_{12} \mathbf{u}_{b,1}} d\mu(\mathbf{U}_a) d\mu(\mathbf{U}_b)$$

with $\mu(\cdot)$ being the Haar measure of the orthogonal group, $\theta_a, \theta_b \in \mathbb{R}^+$ and $\|\mathbf{C}_{kl}\|_\infty < \infty \forall k, l$. Furthermore, assume that the 2×2 block matrix \mathbf{Z} is R-cyclic in the sense of [11].

$$\mathbf{Z} = \begin{pmatrix} \mathbf{C}_{11} & \mathbf{C}_{12} \\ \mathbf{C}_{12}^T & \mathbf{C}_{22} \end{pmatrix}$$

Then, $I_N(\{\theta_k\}, \mathbf{Z})$ is asymptotically solved by:

$$\lim_{N \uparrow \infty} I_N(\{\theta_k\}, \mathbf{Z}) = \exp \left\{ -\frac{N}{2} \int_0^1 \text{tr} \left\{ R_{\mathbf{Z}}^{\mathcal{D}_2}(-\mathbf{P}w) \mathbf{P} \right\} dw \right\}$$

where $\mathbf{P} = \text{diag}\{2\theta_a, 2\theta_b\}$ and $R_{\mathbf{Z}}^{\mathcal{D}_2}(\cdot)$ is the operator valued R-transform of \mathbf{Z} on the algebra of 2×2 diagonal matrices: \mathcal{D}_2 .

Claim 1 (Extension to Rank- ν): Proposition 1 extends to the case of finite rank $\nu > 1$ by the same argument as the Free Fourier Transform extends to rank $\nu \leq \rho\sqrt{N}$ for finite ρ . To reduce notational overhead, the mathematical definition is given in conjunction with Claim 2.

Claim 2 (Modification of the Operator Valued Free Fourier Transform): The modification of the Free Fourier Transform holds also in the Operator Valued Case. Consider a rank ν spherical integral of form:

$$I_N(\{\theta_{k,r}\}, \mathbf{Z}) = \int \prod_{r=1}^{\nu} e^{-N\theta_{a,r} \mathbf{u}_{a,r}^T \mathbf{C}_{11,r} \mathbf{u}_{a,r}^T} \times e^{-N\theta_{b,r} \mathbf{u}_{b,r}^T \mathbf{C}_{22,r} \mathbf{u}_{b,r} - 2N\sqrt{\theta_{a,r}\theta_{b,r}} \mathbf{u}_{a,r}^T \mathbf{C}_{12,r} \mathbf{u}_{b,r}} d\mu(\mathbf{U}_a) d\mu(\mathbf{U}_b)$$

Extending all assumptions of Proposition 1 to accommodate $\nu > 1$, the integral is asymptotically solved by:

$$\begin{aligned} \lim_{N \uparrow \infty} I_N(\{\theta_{k,r}\}, \mathbf{Z}) \\ = \exp \left\{ -\frac{N}{2} \sum_{r=1}^{\nu} \int_0^1 \text{tr} \left\{ R_{\mathbf{Z}_r}^{\mathcal{D}_2}(-\mathbf{P}_r w) \mathbf{P}_r \right\} dw \right\} \end{aligned}$$

Based on Claim 1, we are able to approximate Ξ_X with sufficiently low error at large M and N . Notably, the operator valued condition is only required for the $r = 1$ terms as $\mathbf{Z}_r \forall r > 1$ is diagonal with free on-diagonal entries [11]. The trace of $R_{\mathbf{Z}_r}^{\mathcal{D}_2}$ collapses hence on the sum of scalar R-transforms for all $r > 1$.

$$\begin{aligned} \Xi_X \doteq \exp \left\{ -\frac{\alpha N}{2} \int_0^1 \text{tr} \left\{ R_{\mathbf{Z}}^{\mathcal{D}_2}(-\alpha \mathbf{P}_1 w) \mathbf{P}_1 \right\} dw \right\} \\ \times \exp \left\{ -\alpha N(t-1) \sum_{k \in \{a,b\}} \int_0^1 \theta_{k,2} R_{XJX}(-2\alpha w \theta_{k,2}) dw \right\} \end{aligned} \quad (39)$$

$R_{XJX}(\cdot)$ is the R-transform of $\frac{1}{M} \tilde{\mathbf{X}}_k^T \mathbf{H}_k^T \mathbf{H}_k \tilde{\mathbf{X}}_k$. While a closed-form solution of $R_{XJX}(\cdot)$ exists, the operator valued $R_{\mathbf{Z}}^{\mathcal{D}_2}(\cdot)$ does not admit an analytic form. It is however possible to compute its Taylor expansion around t up to t^2 , which we once again omit to keep the notation compact. The submatrices of \mathbf{Z} as well as the θ values are functions of the eigenvalues of $\mathbf{V}_a^T \mathbf{V}_a$ and $\mathbf{V}_b^T \mathbf{V}_b$. The same holds for the log-determinant terms originating from the gaussian integrals. Hence, the subshell definition in (22) remains unchanged and so do the subshell-density terms $\mathcal{I}(\mathbf{Q}_k) \forall k \in \{a,b\}$. The Taylor expanded terms are reordered to their scaling in β as indicated in (40).

$$f_Z^{\text{RS}}(\beta, t) \propto \int e^{-t\mathcal{B}^{(0)} - t\beta\mathcal{B}^{(1)} - t^2\beta^2\mathcal{B}^{(2)} + \Omega(t^3)} \prod_k dP_k^{\text{RS}} \quad (40)$$

The computation of the mean and variance is structurally identical to (36) and (37). In fact we observe that $\mathcal{B}^{(1)} = \mathcal{B}_a^{(1)} + \mathcal{B}_b^{(1)}$, the coupled spin glass decouples in the first cumulant. The same does not apply to $\mathcal{B}^{(2)}$ which is to be expected since the mean (8) decouples and the variance (9) does not.

IV. RESULTS

To verify that the replica computations produce correct results, the computed metrics are cross-validated to numerical values by Monte Carlo simulation. Throughout this comparison

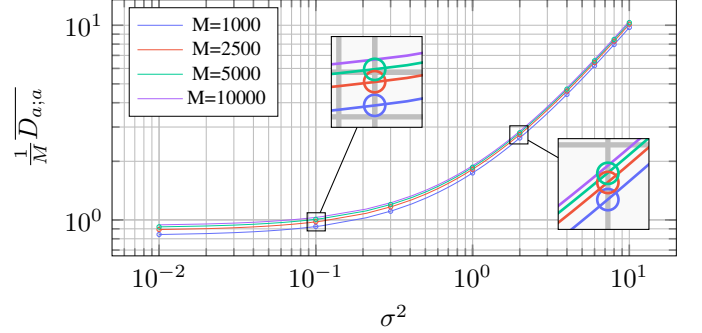


Fig. 3: $\frac{1}{M} D_{a;a}$ over σ^2 at $\alpha = 1$

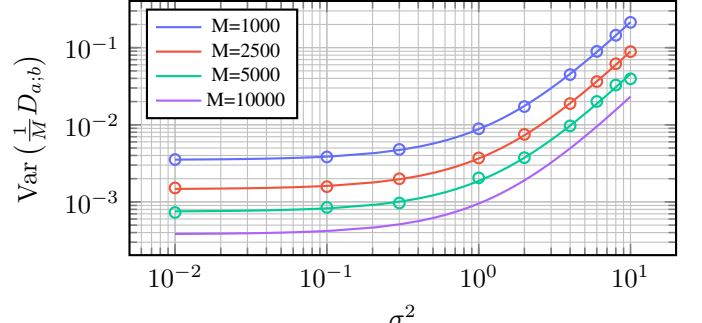


Fig. 4: $\text{Var}(\frac{1}{M} D_{a;b})$ over σ^2 at $\alpha = 1$

we plot the replica computation results as solid lines and the Monte Carlo simulations as markers. In Fig. 3 and Fig. 4 the mean of the normalized squared distance to the DH and the variance of the normalized squared distance to the CH are plotted, respectively. The numerical experiment is conducted for $M \in \{1000, 2500, 5000\}$ and $\alpha \in \{1, 10\}$. Equations (36) and (37) predict the simulated values near perfectly. For $M = 1000$ we carried out a total of 10^4 Monte Carlo simulations whereas a minimum of 3500 and 500 simulations are conducted for $M = 2500$ and $M = 5000$, respectively due to the increased computational complexity. As the room dimension M increases the $L2$ -Norm exhibits reduced ability to discriminate between near and far points [13]. This explains why the mean squared distance in Fig. 3 converges to some value while the corresponding variance decreases as M increases. Furthermore, we note that the double logarithmic plots can be split into two areas. For $\sigma^2 > 1$, both the mean and variance increase near linearly, with gradient one. For $\sigma^2 < 1$, the mean and variance approach a constant which is equal to the values obtained in a hypothetical noise-free system. The average accuracy (7) is approximated by the partial integral over the moment-matched gaussian (41).

$$\overline{\text{AC}_a} \approx \int_{-\infty}^0 \mathcal{N}(D_a; \overline{D_a}, \text{Var}(D_a)) dD_a \quad (41)$$

Figure 5 and 6 depict the obtained estimate and simulated values at $\alpha = 10$ and $\alpha = 1$, respectively. The gaussian approximation is able to predict the phase transition form accuracy 0.5 ($1 - \text{AC}_a = 0.5$), i.e. random classification, to near perfect classification in satisfactory detail. In the asymptotic regime $\sigma^2 \rightarrow 0$, the NCHC exhibits an error floor depending on the room dimension M for constant α . The error floor is not visible for $M = 10000$ at $\alpha = 10$ and $M > 1000$ for $\alpha = 1$ due to too limited numeric precision. Furthermore, we observe a mismatch between the Monte Carlo simulation and replica computations at low misclassification rates. This is due to the maximum number of simulations: 10^4 ; limiting the

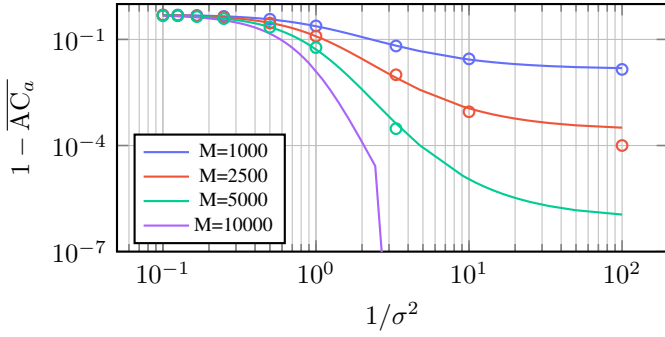


Fig. 5: $1 - \overline{AC}_a$ over $\frac{1}{\sigma^2}$ at $\alpha = 10$

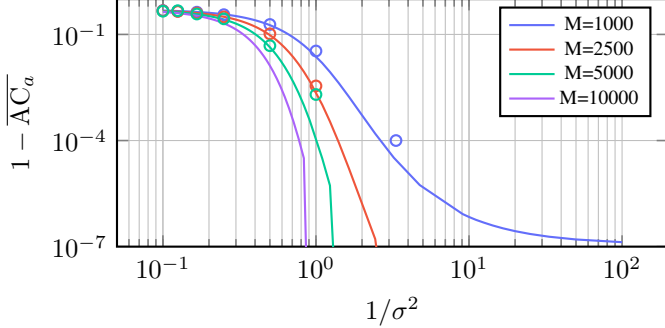


Fig. 6: $1 - \overline{AC}_a$ over $\frac{1}{\sigma^2}$ at $\alpha = 1$

error resolution to 10^{-4} . For $M = 5000$ and $\alpha = 1$ the error accuracy limited to $2 \cdot 10^{-3}$. As α increases, i.e. the length of the training sequence decreases, the critical SNR $1/\sigma_c^2$ at which the phase transition occurs increases and the error floor rises. This implies that low SNR may be compensated by an increased training sequence length and that the error floor is dependent on the number of training samples as it is induced by a sub-optimal sampling of the convex hull. More notable however, higher noise power can be mitigated by increasing the number of antennas M . A similar effect emerges in the heatmap of Fig. 7. For constant N , increasing the room dimensions M reduces the error rate. This behavior might seem unintuitive at first, but can be explained twofold. Firstly, consider that the overlap of the ellipsoids (Fig. 2 (c)) is asymptotically governed by the singular values of \mathbf{H}_a and \mathbf{H}_b in the vicinity of 0, as the two channel matrices are free and hence do not share a preferred direction. The relative overlap area therefore asymptotically tends to zero. In other words: the probability of encountering a sample in the ambiguous area vanishes as $M \uparrow \infty$. Apparently this effect is stronger than the finite sample size effect.

Secondly, the number of users is constant while the number of antennas, i.e. the degrees of freedom (DoF) are increased, allowing for better classification performance. This is not guaranteed to hold if the number of users were to grow in conjunction with the number of antennas.

V. CONCLUSION

In this work, NCHC is applied to blind user identification in a massive MIMO system. The BS is able to identify two UEs by comparing a received signal to $2N$ previously recorded transmissions of known origin without knowledge on their modulation format, coding, CSI or noise power. The misclassification rate at finite, but large, number of antennas M and training sequence length N exhibits an error floor which decreases as M or N are increased. The NCHC is analyzed by the use of replica method for large but finite

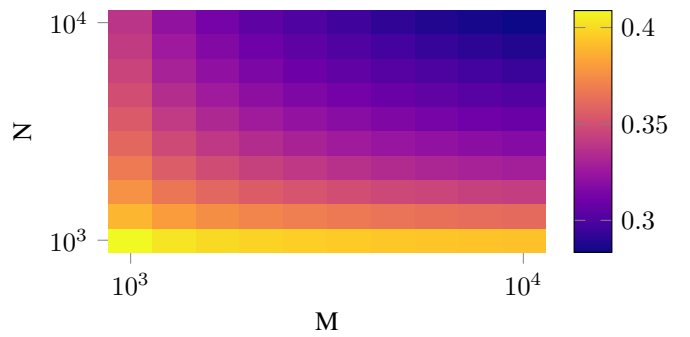


Fig. 7: $1 - \overline{AC}_a$ over M and N at $\sigma^2 = 5$

system size utilizing the inverse temperature β as the large parameter. We postulate the existence of an Operator Valued Free Fourier Transform based on an omitted partial proof. The replica results are verified to numeric simulations which indicate that this proposition is correct. Future work includes but is not limited to: replica computations at the limit $M \uparrow \infty$ as $\alpha = \text{const}$, providing a proof of the Operator Valued Free Fourier Transform, scaling the number of users with the number of antennas and comparing the NCHC to the Bayes Optimal Classifier and the ANCHC.

ACKNOWLEDGMENT

The authors would like to thank Roland Speicher for discussions on the operator valued R-transform, guidance on the corresponding computations and enabling a visit to the Department of Mathematics at Saarland University.

REFERENCES

- [1] S. Zhang, "An Overview of Network Slicing for 5G," *IEEE Wireless Communications*, vol. 26, no. 3, pp. 111–117, Jun. 2019.
- [2] W. Wu, C. Zhou, M. Li, H. Wu, H. Zhou, N. Zhang, X. S. Shen, and W. Zhuang, "AI-Native Network Slicing for 6G Networks," *IEEE Wireless Communications*, vol. 29, no. 1, pp. 96–103, Feb. 2022.
- [3] G. Nalbantov, P. Groenen, and C. Bioch, "Nearest convex hull classification," Econometric Institute, Erasmus University Rotterdam, Tech. Rep., 2006.
- [4] A. Blum, S. Har-Peled, and B. Raichel, "Sparse Approximation via Generating Point Sets," *ACM Transactions on Algorithms*, vol. 15, no. 3, pp. 1–16, Jul. 2019.
- [5] M. Mezard, G. Parisi, and M. Virasoro, *Spin Glass Theory and Beyond: An Introduction to the Replica Method and Its Applications*, ser. World Scientific Lecture Notes in Physics. WORLD SCIENTIFIC, Nov. 1986, vol. 9.
- [6] Harish-Chandra, "Differential Operators on a Semisimple Lie Algebra," 1957.
- [7] C. Itzykson and J.-B. Zuber, "The planar approximation: Part II," in *The Large N Expansion in Quantum Field Theory and Statistical Physics*. WORLD SCIENTIFIC, Aug. 1993, pp. 605–615.
- [8] A. Guionnet and M. Maïda, "A Fourier view on the R-transform and related asymptotics of spherical integrals," *Journal of Functional Analysis*, vol. 222, no. 2, pp. 435–490, May 2005.
- [9] V. A. Marčenko and L. A. Pastur, "Distribution of Eigenvalues for some Sets of Random Matrices," *Mathematics of the USSR-Sbornik*, vol. 1, no. 4, pp. 457–483, Apr. 1967.
- [10] R. R. Müller, "Random matrices, free probability and the replica method," in *2004 12th European Signal Processing Conference*, Sep. 2004, pp. 189–196.
- [11] R. Speicher, "Free Probability Theory," 2009, version Number: 1.
- [12] A. Bereyhi, R. R. Müller, and H. Schulz-Baldes, "Statistical Mechanics of MAP Estimation: General Replica Ansatz," *IEEE Transactions on Information Theory*, vol. 65, no. 12, pp. 7896–7934, Dec. 2019.
- [13] C. C. Aggarwal, A. Hinneburg, and D. A. Keim, "On the Surprising Behavior of Distance Metrics in High Dimensional Space," in *Database Theory — ICDT 2001*, G. Goos, J. Hartmanis, J. Van Leeuwen, J. Van Den Bussche, and V. Vianu, Eds. Berlin, Heidelberg: Springer Berlin Heidelberg, 2001, vol. 1973, pp. 420–434, series Title: Lecture Notes in Computer Science.